Neuron, Vol. 20, 1243–1253, June, 1998, Copyright ©1998 by Cell Press

Cytosolic Ca^{2+} Acts by Two Separate Pathways to Modulate the Supply of Release-Competent Vesicles in Chromaffin Cells

C. Smith,*‡ T. Moser,*‡† T. Xu,* and E. Neher*
*Department of Membrane Biophysics
Max-Planck-Institute for Biophysical Chemistry
Am Fassberg 11
D-37077 Göttingen
Germany
†ENT-Unit
University of Göttingen Medical School
D-37074 Göttingen
Germany

Summary

Recovery from depletion of the readily releasable pool of vesicles (RRP) in adrenal chromaffin cells was studied at differing basal $[Ca^{2+}]_i$ or following protein kinase C (PKC) activation by phorbol esters. Following depletion, the pool size was estimated at varied times from cell capacitance jumps in response to paired depolarizations. The experimentally observed RRP recovery time course and steady-state size could be predicted from the measured $[Ca^{2+}]_i$ signal assuming a Michaelis-Menten-type regulation of the vesicle supply by Ca^{2+}. An elevated recruitment activity was observed at increased $[Ca^{2+}]_i$ even when protein kinase C was blocked, but maximum effects could be obtained only after stimulation of PKC by phorbol esters or by prolonged elevations in $[Ca^{2+}]_i$. We suggest that, in chromaffin cells, elevated cytosolic Ca^{2+} modulates exocytotic plasticity via PKC-dependent and -independent pathways.

Introduction

Both neuroendocrine cells and presynaptic nerve terminals undergo stimulus-dependent changes in their exocytic response to a given stimulation. Neuroendocrine cells display secretory depression following intense stimulation (Neher and Zucker, 1993; Thomas et al. 1993; Horrigan and Bookman, 1994; Moser and Neher, 1997), augmentation following elevation of cytosolic calcium ($[Ca^{2+}]_i$) to submicromolar levels (Bittner and Holz, 1992; von Rüden and Neher, 1993; Thomas et al., 1993), and long-lasting potentiation upon pharmacological activation of protein kinases (Knight and Baker, 1983; Ämmälä et al., 1994; Vitale et al., 1995; Gillis et al., 1996). As in the neuromuscular junction (Elmqvist and Quastel, 1965; Betz, 1970), secretory behavior of endocrine cells can be simulated by sequential secretion models that assume trafficking of exocytotic vesicles between at least one reserve pool and a readily releasable pool (RRP), from which exocytosis occurs (Heinemann et al., 1993; Thomas et al., 1993; Heinemann et al., 1994). The amount of exocytotic release is determined by the number of release-ready vesicles (RRP size) and the probability of each vesicle to undergo exocytosis. Exocytosis in single neuroendocrine cells can be monitored directly both by patch-clamp measurements of exocytotic membrane capacitance changes and electrochemical detection of the released vesicle contents (reviewed in Chow and von Rüden, 1995; Gillis, 1995). Thus, different from synapses, analysis is not complicated by postsynaptic effects. For these reasons neuroendocrine cells have served as a well-suited system to investigate the mechanisms of exocytotic plasticity.

In bovine adrenal chromaffin cells, increases in the RRP size both by $[Ca^{2+}]_i$ (von Rüden and Neher, 1993) and by pharmacological activation of PKC (Gillis et al., 1996) have been described. The goal of the present study was to elucidate the kinetic basis of such exocytotic plasticity and to refine a model describing these processes. Moreover, since activation of PKC by elevated $[Ca^{2+}]_i$ has been demonstrated in chromaffin cells (TerBush et al., 1988), we wanted to test the possibility that at least part of the augmentory effect of elevated $[Ca^{2+}]_i$ might be mediated by Ca^{2+} activation of PKC. We have studied the recovery of the RRP from depletion at differing basal $[Ca^{2+}]_i$, as well as following protein kinase C activation by phorbol 12-myristate 13-acetate (PMA). To do so we probed the RRP size at different times after pool depletion using paired depolarizations (Gillis et al., 1996; Moser and Neher, 1997). Exocytosis was monitored by means of combined patch-clamp measurements of cell membrane capacitance (Cm, an index of vesicle-membrane fusion) and amperometric detection of released catecholamines. Average $[Ca^{2+}]_i$ was recorded using the calcium indicator fura-2. A computer simulation of the experimental protocol, based on a two-step model of secretion (Heinemann et al., 1993), was used to estimate the rate constants of vesicle trafficking to and from the RRP. Under all experimental conditions RRP recovery from depression could be modeled from the measured average $[Ca^{2+}]_i$ assuming a Michaelis-Menten-type Ca^{2+}-dependent regulation of the recruitment of vesicles to the RRP. In PMA-activated cells the RRP kinetics could be modeled by raising the maximal rate constant of the vesicle supply to the RRP. Moreover, inhibition of PKC reduced, but did not abolish, the effects of high basal $[Ca^{2+}]_i$. We therefore suggest that elevated cytosolic Ca^{2+} promotes vesicle recruitment to the release-ready state both through PKC-dependent and PKC-independent mechanisms.

Results

RRP Recovery in Normal Basal $[Ca^{2+}]_i$

The size of the RRP in chromaffin cells held in the perforated patch configuration was estimated through the use of a dual-pulse protocol (Gillis et al., 1996; Moser and Neher, 1997). The dual-pulse paradigm is designed to elicit and measure secretory depression. From the sum and the ratio of the capacitance increases (ΔCm)

‡These authors contributed equally to this work.

to two identical Ca^{2+} current injections given in rapid succession, an upper limit of the RRP, B_{max}, is derived:

$$B_{max} = S/(1 - R^2) \quad (1)$$

where S represents the sum of the capacitance responses to the first (ΔCm_1) and the second (ΔCm_2) depolarizations, and R is defined as the ratio of ΔCm_2:ΔCm_1. A value less than 1 for R represents secretory depression, presumably due to depletion of the RRP. In experimental analyses a maximum R of 0.6 was used because an accurate estimate of the RRP size is only possible when substantial vesicle depletion occurs (see Gillis et al., 1996, for a detailed description of the dual-pulse protocol and its limitations).

By probing the pool size at varying times after a depleting stimulus, the time course of RRP recovery from depletion can be estimated (Stevens and Tsujimoto, 1995; Moser and Neher, 1997; von Gersdorff and Matthews, 1997). Here we investigated the recovery of the RRP size in chromaffin cells by stimulating cells with the dual-pulse protocol at various intervals, as shown in Figure 1A. In response to the first pulse, cell capacitance in this case increased by approximately 192 fF but showed almost no increase in response to the second pulse. The secretory activity measured by the capacitance technique was confirmed in the amperometric record. The large amperometric response to the first pulse, but small response to the second, is consistent with strong secretory depletion, leaving few vesicles in the release-ready state for the second stimulus to act on. About 9 s later the cell was again stimulated through a dual-pulse stimulus. A smaller response was measured to the second dual-pulse. This indicated that the RRP was not able to recover to a very large extent during the 9 s interval. The same cell was stimulated multiple times, with varying intervals between the dual-pulse stimuli (shown in Figure 1B) and values S, R, and B_{max} were calculated for each dual-pulse pair. The plot of the B_{max} values versus the time intervals is shown in Figure 1C.

Analyses like that shown in Figure 1C were carried out on 36 cells, with their pooled data displayed in Figure 2. The result of a computer simulation of the RRP recovery, based on the average measured $[Ca^{2+}]_i$, overlays the data points in Figure 2 (see Experimental Procedures for a description of the simulation). In order to fit the data, the simulation held some model parameters constant. The basal $[Ca^{2+}]_i$ was 280 nM, a mean value measured from fura-2 loaded cells. This value is somewhat higher than the normal resting $[Ca^{2+}]_i$, which prior to stimulation was approximately 150 nM, because $[Ca^{2+}]_i$ increases with repetitive stimulation and incomplete Ca^{2+} clearance. For the simulation a $[Ca^{2+}]_i$ decay time constant of 5.5 s was used, a number measured from fura-2 loaded cells. The peak $[Ca^{2+}]_i$ following a stimulus was about 1.2 μM. The size of the reserve pool A was fixed to be equivalent to 5 pF; further parameters and constants are as described in Experimental Procedures.

In the experiments it was rare to completely exhaust the RRP through electrical stimulation, meaning that the starting point of pool B recovery was higher than 0 fF (a completely exhausted pool). The value of the starting

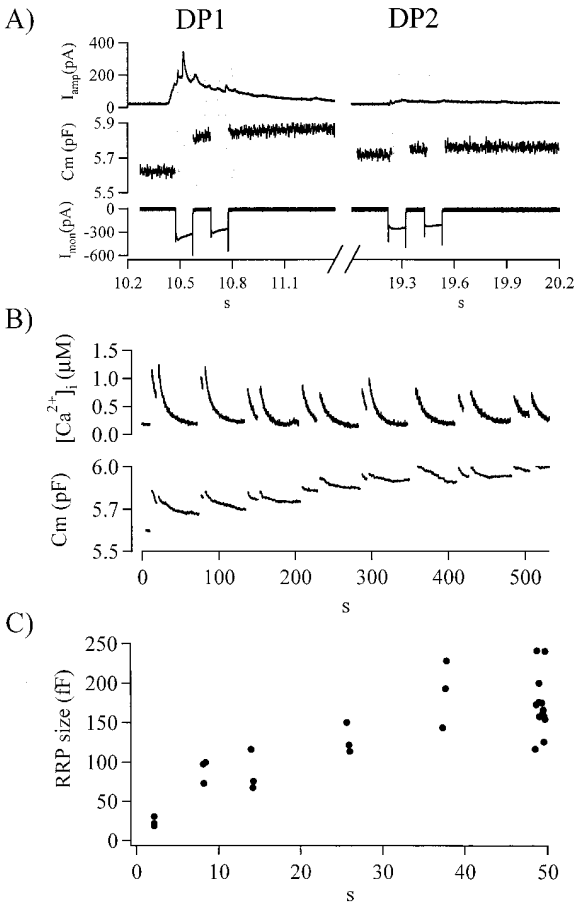

Figure 1. RRP Recovery Measured by a Double Pulse Protocol

Cells were held in the perforated patch voltage clamp at −83 mV. (A) Changes in amperometric currents, cell capacitance, and evoked membrane currents were simultaneously measured in response to stimulation by a dual-pulse protocol. Potentials were adjusted to match as closely as possible the elicited current injections for the pair of depolarizations, but see Gillis et al., 1996, for a detailed description of the limitations of the protocol. The first dual-pulse stimulus (DP1) gave rise to a ΔCm_1 value of 190 fF and a ΔCm_2 value of 2 fF, resulting in a sum response, S, of 192 fF and a ratio, R, of 0.01 (an exceptional degree of depletion, the mean measured R from DP1 in similar conditions was 0.34 ± 0.02). The Cm change measured from DP1 predicted a B_{max} of 192 fF and was accompanied by a large amperometric response. Also in (A) is the evoked inward current, mostly representing Ca^{2+} influx. The second dual-pulse stimulus (DP2) was applied 8.7 s after the first and resulted in a much smaller secretory response, with an S of 32 fF and an R of 0.72, predicting a B_{max} value of 68 fF.

(B) Low time resolution plot of cell capacitance and Ca^{2+} calculated from fura-2 fluorescence of the cells. Many pairs of variably spaced dual-pulse stimuli were applied to single cells. Adequate time for full RRP recovery was allowed prior to a new pair of dual-pulse stimuli.

(C) Plot of B_{max} values versus the time interval before stimulation. Pairs of dual-pulse stimuli that were likely to provide accurate estimates of B_{max} were identified based on the values S and R from DP1 (S_1 and R_1 respectively). A minimum value of 40 fF was chosen for S_1, with lesser responses considered prone to measuring error from an unfavorable signal-to-noise ratio. A value of 0.6 for R_1 was required in order to ensure adequate depletion of the RRP and estimation of B_{max}. S and R values for DP2 were also measured and B_{max} calculated from Equation 1 was plotted against the time interval.

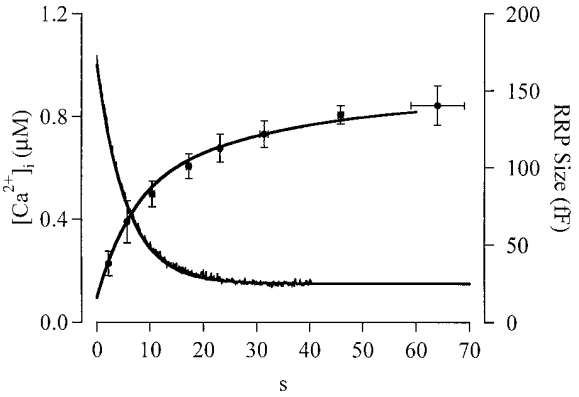

Figure 2. Measured and Simulated RRP Recovery

The time course of RRP recovery was measured as described in Figure 1 for 36 cells and is plotted (filled circles). The data were binned according to the DP1-DP2 interval for clarity in presentation. Also plotted is an ensemble average of 7 representative postdepolarization Ca^{2+} decay transients as measured from fura-2-loaded cells. The time course of RRP recovery was modeled in a computer simulation based on the "two-step model of secretion control" (Heinemann et al., 1993, see description in Experimental Procedures). The results from the simulation are plotted as solid lines. Input parameters for the model were as follows: basal $[Ca^{2+}]_i$ = 280 nM, Ca^{2+} decay time constant = 5.5 s, $[Ca^{2+}]_i$ immediately following stimulation = 1.2 μM, constant $a_1 = 0.007\ s^{-1}$, rate constant $k_{-1} = 0.031\ s^{-1}$, $a_3 = 0.035\ \mu M^{-3}\ s^{-1}$, size of pool A = 5 pF, initial post stimulus pool B (B_{int}) = 16 fF, b_1 = 1.9 μM.

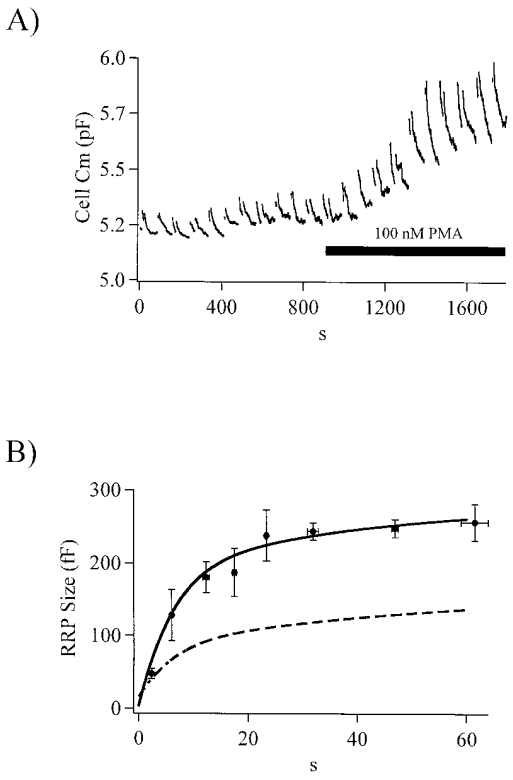

Figure 3. PMA Increases the Initial Rate of RRP Recovery

(A) Membrane capacitance measured from a cell in the perforated patch configuration before and after application of 100 nM PMA is displayed.

(B) B_{max} values from 15 cells treated with 100 nM PMA were calculated and are plotted. The solid line represents a computer simulation fitted to the PMA B_{max} data set. The fitted simulation was achieved using the control input parameters as described in Figure 2, with the exception that a_1 was increased from the control value of 0.007 s^{-1} to 0.014 s^{-1}. For comparison, the simulation of the control condition is also plotted (dashed line).

point was derived from the responses to dual-pulses. The average poststimulus pool B size, here termed B_{int} (for B_{max} intercept at t = 0), can be calculated under the assumption that the second pulse releases the same fraction of the available pool as the first pulse. The value B_{int} is given by

$$B_{int} = B_{max} \cdot R_1^2 \qquad (2)$$

where B_{int} is a function of the ratio R of the depleting dual-pulse stimulation (termed R_1, see the legend to Figure 1) and the maximum pool size B_{max}. Additionally, the K_D for Ca^{2+} of the vesicle recruitment from pool A to B (b_1 from Equation 4), originally taken to be 1.2 μM by Heinemann and colleagues (1993), was changed to 1.9 μM in order to fit the control condition with the simulation. The free parameters left in the simulation, the maximum vesicle supply to pool B, and spontaneous loss from B to A (a_1 and k_{-1}, respectively) were varied until a satisfactory fit was achieved (see Table 2 for a complete summary of simulation parameters). The simulation very well fits the average data, which shows rapid recovery while $[Ca^{2+}]_i$ is high, and a slow approach toward the steady-state value, once $[Ca^{2+}]_i$ has decayed back to baseline.

RRP Recovery in the Presence of PMA

Protein kinase C (PKC) activation has been reported to increase secretory activity in neuroendocrine cells (Knight and Baker, 1983; Ämmälä et al., 1994; Vitale et al., 1995) evidently by increasing the size of the RRP (Gillis et al., 1996). We wanted to examine the PKC effect in order to determine its mode of action. Toward this end, we treated cells in perforated patch voltage clamp with 100 nM phorbol 12-myristate 13-acetate (PMA), an activator of PKC. An example of such an experiment is shown in Figure 3. Data from 15 cells treated by incubation in PMA were pooled and analyzed (Figure 3B). The data could not be fitted with the simulation parameters determined for the control perforated patch data set (Figure 3B, dotted line), unless a_1 (maximum rate constant for the vesicle supply to the RRP) was increased from the control value of 0.007 s^{-1} to 0.014 s^{-1}. The doubling of the constant a_1 resulted in the approximate doubling of the RRP from 140 fF to 260 fF. It therefore seemed that, while retaining a similar time course to that observed under control conditions, PMA appeared to increase the number of vesicles in the release-ready state by raising the rate of vesicle supply to the RRP. The possibility that PMA acted by decreasing the rate of vesicle loss from pool B backward to pool A (represented by the value k_{-1}) seems unlikely since the time course of refilling under PMA was similar to that of the control data. Had PMA increased the RRP size by decreasing k_{-1}, we would have expected to observe a slower time course of RRP recovery (see Equation 13 in Experimental Procedures). It should be mentioned,

however, that a very similar steady-state RRP pool increase can be obtained in the model by lowering the value for b_1 of Equation 4 (increasing the affinity of the Michaelis-Menten binding site). However, this change made it very difficult to obtain a suitable fit to both the rising phase and the plateau level of the RRP size.

RRP Recovery in Low $[Ca^{2+}]_i$

In order to test for the role basal $[Ca^{2+}]_i$ plays in the modulation of the RRP recovery, an experimental protocol was designed to lower the cytosolic Ca^{2+} artificially. Cells were again studied in the perforated patch configuration, but with a slightly altered internal pipette solution. The NaCl of the standard pipette solution was replaced by 9.5 mM CsCl. Additionally, the cells were bathed in a Ringer that contained no added $CaCl_2$ with the intention of increasing the cell Na^+ gradient and decreasing the Ca^{2+} gradient, thereby increasing the efficiency of Ca^{2+} removal from the cytosol through Na^+-dependent Ca^{2+} clearance. Then, just prior to the dual-pulse stimulus, Ringer containing 20 mM $CaCl_2$ was puffed onto the cell through a local puffer pipette to allow stimulus-evoked Ca^{2+} influx capable of supporting secretion (shaded region, Figure 4A). Using fura-2-loaded cells, it was estimated that the basal $[Ca^{2+}]_i$ was lowered from the control mean value of 280 nM to approximately 72 nM. When the experimental dual-pulse protocol was applied to these cells, it was observed that the steady-state RRP had decreased in size from a control value of 140 fF to 51 fF. Additionally, the RRP recovery in the lowered $[Ca^{2+}]_i$ passed through a maximum of 75 fF after 20 s before decreasing to the steady-state size. This observation can be explained as a overfilling of the RRP shortly after the stimulus while $[Ca^{2+}]_i$ is high. As $[Ca^{2+}]_i$ falls, the Ca^{2+}-dependent vesicle supply to the RRP (described by the Ca^{2+}-dependent rate constant k_1) decreases, allowing the Ca^{2+}-insensitive loss of vesicles from the RRP (described by the rate constant k_{-1}) to dominate, leading to shrinkage of the RRP to its smaller steady-state size. Therefore, two phases of refilling could be distinguished, a robust phase during the elevated Ca^{2+} following stimulation, and a relaxation toward an equilibrium RRP size at resting Ca^{2+}. The experimentally observed recovery time course could be matched by the simulation using the same parameters as those of Figure 2 except for taking into account the lower basal $[Ca^{2+}]_i$ (72 nM; Figure 4B)

RRP Recovery in Elevated $[Ca^{2+}]_i$

Similar to the PMA effect, increased cytosolic Ca^{2+} concentrations have been indicated as exerting a positive influence on the secretory response in chromaffin cells (Bittner and Holz, 1992; von Rüden and Neher, 1993), an effect we observed as well in the present study. In some cells the basal $[Ca^{2+}]_i$ rose late in experiments, due mainly to seal instability or cell leakage. In such cases we observed under the increased basal $[Ca^{2+}]_i$ (Figure 5A) that the secretory responses became larger, as is predicted by the two-step model (Heinemann et al., 1993; Neher and von Rüden, 1994; see Figure 6A). For a more detailed examination of the role of calcium, we buffered the basal $[Ca^{2+}]_i$ of cells to specific levels

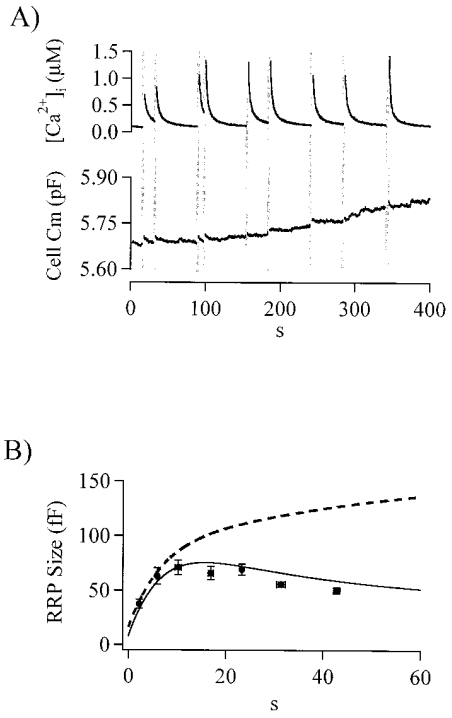

Figure 4. Lowered Cytosolic Ca^{2+} Alters the RRP Recovery

(A) Basal cytosolic Ca^{2+} concentrations in chromaffin cells held in the perforated patch configuration were lowered through a combination of low internal Na^+ and low external Ca^{2+}. The dual-pulse protocol described in Figure 1 was applied to these cells, with measured cytosolic Ca^{2+} and cell Cm plotted. Immediately prior to stimulation, Ringer containing 20 mM $CaCl_2$ was puffed locally onto the patched cell, indicated by the shaded regions.

(B) B_{max} values from 28 cells studied with this protocol were calculated as described for Figure 1 and are plotted (filled circles). Also plotted is the result from the computer simulation (solid line) for which the input parameters were identical to those described in Figure 2, except that basal Ca^{2+} was set to 72 nM. For comparison, the simulation of the control condition is also plotted (dashed line).

in whole-cell recordings and studied the RRP size and recovery behavior. This was achieved by balancing the Ca^{2+} buffer fura-2 with various levels of free Ca^{2+} in the whole-cell pipette solution. The Ca^{2+} buffer pipette solution differed from the standard whole-cell solution only in that it contained the Ca^{2+}/fura-2 combinations shown in Table 1. In all cases the final free fura-2 concentration was approximately 50 μM.

Qualitatively, raising $[Ca^{2+}]_i$ from 100 nM to approximately 500 nM increased the secretory response significantly (Figure 5B, i and ii), while further increases of $[Ca^{2+}]_i$ caused elevated asynchronous release, and an accompanied decrease in the evoked response (Figure 5B, iii). This supports experimentally the increase of steady-state RRP size as a function of $[Ca^{2+}]_i$ (Figure 6A, filled circles) as predicted by the two-step model. Using the same input parameters as were used for the computer simulation shown in Figure 2, we calculated the predicted steady-state RRP size as dependent upon the cytosolic Ca^{2+} concentration (Figure 6A, dotted line). At low $[Ca^{2+}]_i$, the model predicts an increase in RRP size with increasing $[Ca^{2+}]_i$ as the rate of vesicle recruitment to pool B increases. At a certain point, however,

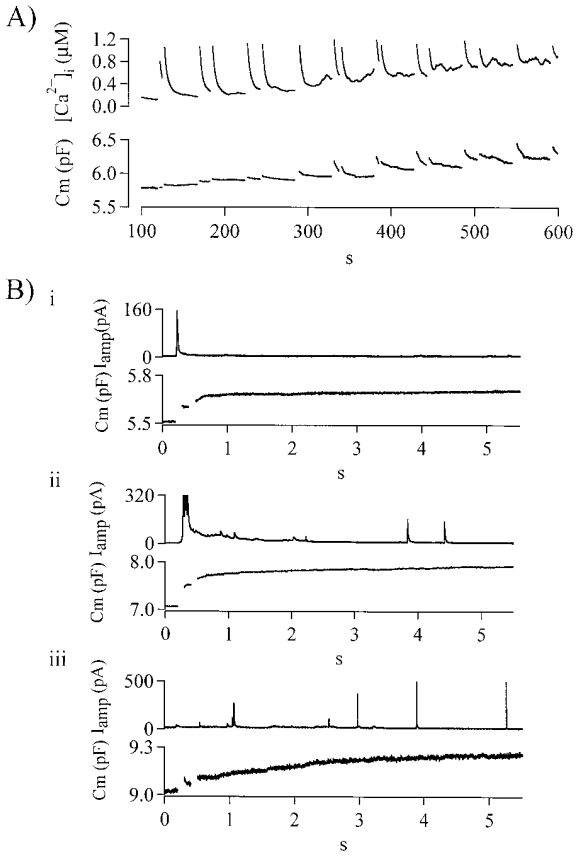

Figure 5. Comparison of Evoked Secretion at 3 Different Basal Ca^{2+} Concentrations

(A) Cm and $[Ca^{2+}]_i$ measured from a cell where basal Ca^{2+} slowly rose during the experiment are plotted. As $[Ca^{2+}]_i$ increased, so did the size of the measured secretory response.

(B) Whole cell recordings in which the basal $[Ca^{2+}]_i$ was buffered to different levels between 100 and 1000 nM showed differing secretory activities. (i) A cell with low cytosolic Ca^{2+} measured to be 110 nM was stimulated with the dual-pulse protocol. Evoked Cm increases and amperometric currents were modest in magnitude. (ii) A cell with a measured basal $[Ca^{2+}]_i$ of about 600 nM; evoked Cm increases and amperometric currents were greatly increased (note that the amperometric axis in [ii] is truncated at 320 pA although the current reached a maximum of ~720 pA). (iii) Cytosolic Ca^{2+} raised to even higher concentrations (in this example about 1200 nM) showed a decreased evoked Cm increase with respect to the record in (ii). However, the poststimulus amperometric and Cm records in (iii) indicate that the frequency of nonevoked exocytotic events is increased.

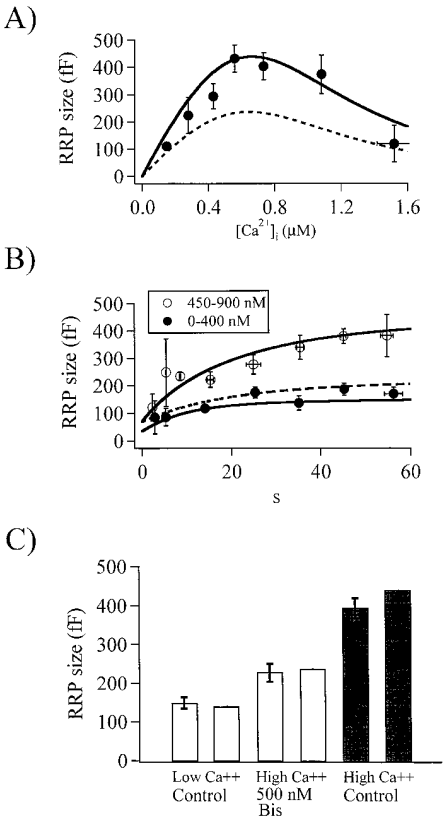

Figure 6. Raised $[Ca^{2+}]_i$ Effects Steady-State RRP Size and Recovery

(A) Measured B_{max} values collected from 102 cells measured in the whole-cell configuration where the basal $[Ca^{2+}]_i$ had been buffered to differing levels were pooled and are plotted versus measured basal Ca^{2+} concentrations (filled circles). The simulation of the steady-state RRP size with the input parameters described for the control RRP recovery model in Figure 2 (dashed line), or with the constant a_1 as determined for the PMA-treated cells in Figure 3 (solid line).

(B) The time dependence of RRP recovery was measured for cells that had basal $[Ca^{2+}]_i$ buffered to values between 0 and 450 nM, and 450 and 900 nM. The simulation for the lower Ca^{2+} range (lower solid line) was calculated using the simulation input parameter described for the control data set (Figure 2) with basal Ca^{2+} set to 297 nM. A second simulation (dashed line) with the control input parameters was run where the basal $[Ca^{2+}]_i$ was set to 594 nM (average $[Ca^{2+}]_i$ for the 450–900 nM data group) but did not approximate the measured data. If Ca^{2+} activation of PKC was assumed, and the elevated a_1 value from the simulation fitted to the PMA-treated cell was used (Figure 3, $a_1 = 0.014\ s^{-1}$), the data could be well approximated (upper solid line).

(C) Plotted are the measured (left bars) and simulated (right bars) steady-state RRP sizes of cells with Ca^{2+} buffered to different levels and at high Ca^{2+} after treatment with BIS. In low Ca^{2+} control cells, the measured RRP pool size (148.7 ± 15 fF) could be simulated by assuming the measured mean $[Ca^{2+}]_i$ (141 ± 6.6 nM) and the control rate constant a_1 (0.007 s^{-1}). Similarly in high $[Ca^{2+}]_i$ cells (681 ± 16 nM) that had been treated with 500 nM BIS, the measured RRP size (227 ± 23 fF) could be simulated assuming the control rate constant a_1. In cells with intact PKC activity and $[Ca^{2+}]_i$ buffered to high levels (695 ± 8 nM), the RRP (392 ± 26 fF) could only be simulated by assuming the elevated rate constant a_1 predicted from the PKC-activated cells (0.014 s^{-1}).

vesicle flow away from pool B dominates, as the rate of exocytosis increases steeply. Clearly, this prediction, that RRP size should go through a maximum as $[Ca^{2+}]_i$ increases was confirmed by the data (Figure 6A). However, the degree to which this occurs was underestimated, especially at higher concentrations of Ca^{2+}. Therefore, we asked whether the increased RRP in elevated Ca^{2+} was due only to the direct Ca^{2+}-dependency of k_1 or if it also resulted from a secondary mechanism such as an increase in the rate constant a_1 by Ca^{2+}-activated PKC. When, accordingly, we simulated the RRP size with the elevated constant a_1 previously used for the PMA activated cells (0.014 s^{-1}), the simulated

Table 1. Whole-Cell Ca^{2+} Buffer Solutions

Final free $[Ca^{2+}]_i$	Added $[Ca^{2+}]$	Added fura-2
100 nM	0 μM	75 μM
300 nM	45 μM	125 μM
500 nM	95 μM	175 μM
700 nM	145 μM	225 μM

RRP size agreed well with the measured data at high Ca^{2+} (Figure 6A, solid line). At lower Ca^{2+} concentrations the points fell below that predicted with the simulation possibly due to an incomplete Ca^{2+}-dependent PKC activation.

The kinetics of RRP recovery were studied in 102 cells under the whole-cell configuration in basal and elevated Ca^{2+}. $[Ca^{2+}]_i$ was buffered to varying levels and pooled data are plotted in Figure 6B. The data were divided into 2 groups, those that had measured $[Ca^{2+}]_i$ lower than 400 nM and those that had $[Ca^{2+}]_i$ between 450 and 900 nM. The recovery time course and steady-state RRP size (140 fF) measured in the lower Ca^{2+} range could be simulated under the control set of assumptions with a Ca^{2+} decay time constant of 7.2 s (measured under similar conditions by Neher and Augustine, 1992) and assigning the basal Ca^{2+} level in the simulation to 297 nM, a value obtained experimentally through fura-2 recordings made during the experiments (Figure 6B, lower solid line).

Cells with $[Ca^{2+}]_i$ buffered to between 450 and 900 nM exhibited an increased RRP (404 fF). Contrary to that described for the 0–400 nM Ca^{2+} condition, the recovery could not be simulated just by assigning the basal Ca^{2+} to the measured average of 594 nM (Figure 6B, dotted line). However, if the elevated $[Ca^{2+}]_i$ was assumed to activate the Ca^{2+}-dependent PKC, raising the rate constant a_1 to the levels obtained under PMA incubation, the high Ca^{2+} data were well fit by the simulation (Figure 6B, upper solid line). It should be possible to test this assumption by inhibiting PKC activity, buffering $[Ca^{2+}]_i$ to an elevated level, and measuring the steady-state RRP size. We buffered $[Ca^{2+}]_i$ to approximately 700 nM in whole-cell patch recordings in the presence of the specific PKC inhibitor bisindolylmaleimide I (BIS, 500 nM in the internal pipette solution). BIS has been shown in chromaffin cells to block effectively phorbol ester activation of PKC and the subsequent increase in RRP size. BIS treatment leaves largely unchanged the RRP in cells at control Ca^{2+} levels and not treated with PMA (Gillis et al., 1996). The size of the RRP measured in cells treated with BIS and with elevated basal $[Ca^{2+}]_i$ is plotted in Figure 6C. For the control low Ca^{2+} condition, measured data (left bar) could be simulated (right bar) by assuming the measured $[Ca^{2+}]_i$ of 141 nM and the control rate constant a_1 of 0.007 s^{-1}. In elevated Ca^{2+}, and in the presence of BIS, the measured data could again be simulated assuming the measured $[Ca^{2+}]_i$ of 681 nM and the control rate constant a_1. But, in high Ca^{2+} and without the addition of BIS, the data could only be simulated by assigning the measured $[Ca^{2+}]_i$ of 695 nM and using the elevated rate constant a_1 measured in the PMA-activated cells (Figure 2) of 0.014 s^{-1}.

Summary of the Simulation Parameters

The results from the 5 simulations representing the different experimental conditions are summarized in Table 2. The values in each column represent simulation parameters resulting in a reasonable fit to the measured data. An initial parameter set for the model was determined by fitting the control perforated patch data set. In most cases, except in the presence of PMA or in highly elevated cytosolic Ca^{2+}, RRP characteristics could be well simulated with the control fit parameters based on the actual Ca^{2+} profile. In cells treated with 100 nM PMA, or when $[Ca^{2+}]_i$ was buffered above approximately 400 nM, a further increase in the peak vesicle supply was required to fit the experimental data with the simulation, presumably due to the Ca^{2+}-dependent, or phorbol ester-dependent, activation of protein kinase C.

Discussion

The identification of the readily releasable pool as a major determinant of exocytotic plasticity has become an important concept in the secretion field. Certain types of secretory plasticity observed in neuroendocrine cells as well as in synapses have been related to modulation of RRP size. Thus, depletion of release-ready vesicles has for a long time been suggested to be a major mechanism for synaptic depression in the neuromuscular junction (Liley and North, 1953; del Castillo and Katz, 1954; Elmqvist and Quastel, 1965; Betz, 1970). Similar conclusions have been drawn for secretory depression in neuroendocrine cells (Heinemann et al., 1993; Thomas et al., 1993) and hippocampal synapses (Stevens and Tsujimoto, 1995).

An enhanced supply of fusion-competent vesicles is believed to underlie accelerated recovery from depression during high frequency stimulation (Kusano and Landau, 1975; von Gersdorff et al., 1997) and might in some preparations contribute to augmentation and posttetanic potentiation (Zucker et al., 1991; Byrne and Kandel, 1996). Yet, so far relatively little is known about the mechanisms by which repeated stimulation might activate the recruitment of release-ready vesicles. There is a close temporal correlation between the elevated cytosolic Ca^{2+} and augmentation as well as posttetanic potentiation (Kretz et al., 1982; Delaney et al., 1989). When the elvation of cytosolic Ca^{2+} during conditioning stimulation is suppressed in crayfish neuromuscular junction, both augmentation and posttetanic potentiation are reduced (Kamiya and Zucker, 1994). Therefore, it has been postulated that the increased cytosolic Ca^{2+} might signal the enhanced vesicle supply to the RRP during repeated stimulation (for review, see Zucker, 1996). In neuroendocrine cells an increased RRP size caused by moderate elevation of $[Ca^{2+}]_i$ has been demonstrated (von Rüden and Neher, 1993). In the present study we confirm and extend the previous results by measuring the steady-state size of the RRP in chromaffin cells with a dual-pulse protocol over a range of $[Ca^{2+}]_i$ (Figures 4–6). We observed a bell-shaped relationship with a peak at a $[Ca^{2+}]_i$ of about 600 nM. The drop in RRP size at higher $[Ca^{2+}]_i$ was most likely due to an increased rate of vesicle fusion (see Figure 6).

Table 2. Summary of Simulation Parameters

	Perforated Patch Control	Perforated Patch low $[Ca^{2+}]_i$	Whole Cell 0–450 nM $[Ca^{2+}]_i$	Whole Cell 450–1200 nM $[Ca^{2+}]_i$	Perforated Patch 100 nM PMA
Basal $[Ca^{2+}]_i$*	280 nM	72 nM	297 nM	594 nM	275 nM
$[Ca^{2+}]_i$ at t = 0*	1.2 μM	1 μM	1.2 μM	1.4 μM	1.2 μM
Ca^{2+} decay τ*	5.5 s	5.5 s	7.2 s	7.2 s	5.5 s
a_3 value*	0.035 $\mu M^{-3}\ s^{-1}$	0.035 $\mu M^{-3}\ s^{-1}$	0.035 $\mu M^{-3}\ s^{-1}$	0.035 $\mu M^{-3}\ s^{-1}$	0.035 $\mu M^{-3}\ s^{-1}$
Pool A size*	5 pF	5 pF	5 pF	5 pF	5 pF
B_{int} value*	16 fF	8 fF	35 fF	70 fF	4 fF
a_1 value†	0.007 s^{-1}	0.007 s^{-1}	0.007 s^{-1}	0.014 s^{-1}	0.014 s^{-1}
k_{-1} value†	0.031 s^{-1}	0.031 s^{-1}	0.031 s^{-1}	0.031 s^{-1}	0.031 s^{-1}
b_1 value†	1.9 μM	1.9 μM	1.9 μM	1.9 μM	1.9 μM

*Obtained from literature or measured in this study.
†Values selected to fit the data in this study.

We further investigated the effects of cytosolic Ca^{2+} on the vesicle trafficking to and from the RRP during the recovery from depression. All experimental conditions resulted in recovery modes that could successfully be modeled on the basis of the measured cytosolic Ca^{2+} signal by the two-step model of Heinemann et al. (1993) that assumes a Ca^{2+}-dependent, Michaelis-Menten-type activation of the recruitment of vesicles to the RRP. Although we do not know the local $[Ca^{2+}]_i$ that actually controls the vesicle supply, it seems reasonable to rely on the measured average $[Ca^{2+}]_i$ mainly because equilibration of Ca^{2+} throughout chromaffin cells (Neher and Augustine, 1992) happens within a small fraction of the time it takes to recover the RRP (about 14 s in the control condition, see Results section and Figure 2).

The present study shows that at least two phases of recovery from secretory depression have to be distinguished. First the short poststimulus period of transient $[Ca^{2+}]_i$ elevation (phase I) and second, the later phase when $[Ca^{2+}]_i$ is close to basal levels (phase II). This biphasic behavior became most evident in experiments where we lowered the basal $[Ca^{2+}]_i$ by enhancing the cellular Ca^{2+} clearance (see Figure 4). Under these conditions we observed a rapid initial increase of pool size during phase I and a decline towards the steady-state RRP value representative of the basal $[Ca^{2+}]_i$ (phase II). This finding provides evidence that at least for short elevations of $[Ca^{2+}]_i$ the activation of the vesicle recruitment to the RRP is reversible, allowing for dynamic pool size changes in response to variations of $[Ca^{2+}]_i$. In chromaffin cells poststimulus $[Ca^{2+}]_i$ decays with a time constant of about 5 to 10 s (Neher and Augustine, 1992; Figure 2 of the present study). Therefore, the $[Ca^{2+}]_i$ transient has significant impact on the RRP recovery even at low stimulation frequencies. This is likely to be different in presynaptic nerve terminals where the $[Ca^{2+}]_i$ transients are much shorter (fractions of seconds; Helmchen et al., 1996). There one would expect, that an augmented recruitment would become evident only at higher frequency stimulation when the initial transiently elevated Ca^{2+} phase gains more impact and basal $[Ca^{2+}]_i$ climbs, respectively. This view is consistent with the above-mentioned close temporal correlation of elevated cytosolic Ca^{2+} and synaptic potentiation (Kretz et al., 1982; Delaney et al., 1989).

For two sets of experiments—high basal $[Ca^{2+}]_i$ and PKC activation by PMA—increasing the maximal rate constant of the recruitment process fit the data with the same Ca^{2+} dependency as for control. Keeping all other parameters constant, recovery under both experimental conditions could be simulated using a maximal vesicle supply rate constant (a_1) of 0.014 s^{-1} instead of 0.007 s^{-1} (see Figures 3 and 6). For the case of PKC activation by PMA, we also tested the possibility of an increased Ca^{2+} sensitivity of the vesicle supply process without a change of the maximal activity. In order to fit the data with a lower K_D for Ca^{2+} (b_1), we had to almost double the rate constant of the vesicle loss (k_{-1}) from the RRP to the reserve pool. Such an increase in k_{-1} is, however, not supported by the data, since the time course of RRP recovery—which is determined by vesicle loss from the RRP (see Equation 13)—was not changed by PMA. The absence of detectable changes in k_{-1} also rules out the possibility that PMA led to a larger RRP by reducing the loss of vesicles back to the reserve pool. Therefore, the most likely explanation of the RRP behavior in PMA-treated cells is that PKC-dependent phosphorylation acts synergistically with Ca^{2+} action to stimulate the supply of vesicles.

Here we show that the increase of the pool size by elevated $[Ca^{2+}]_i$ can in part be blocked by bisindolylmaleimide I (BIS), a blocker of PKC. At a $[Ca^{2+}]_i$ of about 700 nM the RRP, upon inhibition of PKC by 500 nM intracellular BIS I (IC_{50}: 10 nM), dropped from 390 ± 26 fF to 227 ± 19 fF, a value that exceeds the RRP size at low $[Ca^{2+}]_i$ (149 ± 17 fF at 140 nM). Interestingly, it very well matched the number predicted for the steady-state RRP size at 680 nM basal $[Ca^{2+}]_i$ when the standard model parameters were used (236 fF, disregarding PKC effects). These findings lead us to suggest that vesicle supply in chromaffin cells is activated by elevated cytosolic Ca^{2+} through PKC-dependent phosphorylation as well as via a PKC-independent mechanism, which shows a Michaelis-Menten activation by Ca^{2+}. Reversible activation of PKC by elevation of $[Ca^{2+}]_i$ has been demonstrated in chromaffin cells (TerBush et al., 1988) as well as in other neuroendocrine cells (Deeney et al., 1996). In chromaffin cells Ca^{2+} influx caused translocation of PKC to the membranes within only a few seconds. $[Ca^{2+}]_i$ as low as 300 nM was sufficient to cause some PKC translocation, and already a small increase in the amount of membrane-bound PKC caused a massive

enhancement of Ca^{2+}-induced secretion (TerBush et al., 1988). The present study shows that above a certain $[Ca^{2+}]_i$ PKC-dependent phosphorylation activates the recruitment of release-ready vesicles. This phosphorylation-dependent effect appears to reach its maximum value already in the submicromolar range of $[Ca^{2+}]_i$ because the BIS-sensitive RRP increase at a basal $[Ca^{2+}]_i$ of 700 nM (73%) is similar to the rise in RRP size induced by a saturating concentration of PMA (65% at 100 nM) at control basal $[Ca^{2+}]_i$. Interestingly, we could simulate experiments in which the basal $[Ca^{2+}]_i$ was below 300 nM without increasing the maximal rate constant for the period of the poststimulus Ca^{2+} elevation. We cannot exclude that small PKC-dependent effects were obscured by the variance in these data sets. Still, the time of Ca^{2+} elevation following depolarization seems to be too short to cause a significant enhancement of vesicle supply through PKC-dependent phosphorylation.

The BIS-sensitive enhancement of release-ready vesicle supply at elevated basal $[Ca^{2+}]_i$ described here is likely to be of physiological relevance for chromaffin cells as well as for other neurosecretory preparations. Ca^{2+}-dependent PKC activation could potentiate the secretory responses of chromaffin cells at higher spiking frequencies of the splanchnic nerve. Strong enhancement of secretory responses during trains of short depolarizations, indeed, has been observed in chromaffin cells as well as in other neuroendocrine cells (e.g., the threshold phenomenon described for chromaffin cells and neurohypophyseal nerve terminals by the lab of M. Nowycky [Seward et al., 1995; Seward and Nowycky, 1996]). After a number of stimuli, the climbing average $[Ca^{2+}]_i$ would be expected to activate PKC, resulting in larger secretory responses due the increased rate of vesicle supply.

So far it is unclear which steps of a vesicles maturation are observed in our experiments. Moreover, the molecular targets of elevated $[Ca^{2+}]_i$ and PKC that mediate the modulation of the vesicle supply to the RRP are not yet known. Vesicles recruited to the RRP within the observed time window might have already been docked, such that the effects of elevated Ca^{2+} and enhanced PKC activity are on priming of the exocytotic machinery. In fact, the RRP of chromaffin cells determined in electrophysiological experiments might represent only a fraction of the vesicles, which are already located close to the plasma membrane (Parsons et al., 1995; Plattner et al., 1997). On the other hand, it has been suggested that Ca^{2+} and PKC enhance the supply of release-ready vesicles to the plasma membrane by inducing breakdown of the barrier of cortical actin network (Vitale et al., 1995).

There is an entire array of Ca^{2+}-binding proteins that have been implicated in regulation of exocytosis, including synaptotagmins, CAPS, rabphilin-3A, doc2, annexin II, and scinderin (see recent review by Bennett, 1997). A comparison of their Ca^{2+} dependencies to that found here for the recruitment of releasable vesicles is complicated by the fact that they can be influenced by the amount and composition of phospholipids present (e.g., Gerke and Moss, 1997). Beside the PKC-dependent action demonstrated in the present study, elevated cytosolic Ca^{2+} could regulate exocytosis through the activation of other protein kinases as well (Greengard et al., 1993). Molecular targets of PKC which could potentially mediate the observed enhancement of release-ready vesicles to the RRP include p145 (Nishizaki et al., 1992), annexins (Sarafian et al., 1991), the myristoylated alanine-rich C kinase substrate (MARCKS; Hartwig et al., 1992), and munc-18 (Fujita et al., 1996), as well as components of the 20S complex (Shimazaki et al., 1996).

Future experiments will be required to test the effects of the above-mentioned molecules on the recovery kinetic of the RRP. We hope that the results and the approach presented here will prove helpful in these studies. Additional information can be expected to come from optical measurements of intracellular vesicle movement and exocytosis, for example made possible recently by total internal reflection fluorescence microscopy (TIRFM; Steyer et al., 1997; Oheim et al., 1998).

Experimental Procedures

Chromaffin Cell Culture

Chromaffin cells were prepared by digestion of adult bovine adrenal medulla in collagenase type I (0.5 mg · ml^{-1}; Worthington Enzymes, Freehold, NJ) and cultured for 1–4 days. Further details are described in Zhou and Neher (1993). After enrichment on a Percoll gradient, cells were plated in DMEM, 1× GMS-X (a defined serum substitute; GIBCO-BRL, Bethesda, MD), penicillin, and streptomycin at a density of approximately 4.4×10^3 mm^{-2}. Cultures were maintained at 37°C and 10% CO_2.

Solutions

During recordings, cells were constantly superperfused at a rate of approximately 1 ml · min^{-1} with a Ringer solution of the following composition (in mM); 150 NaCl, 10 HEPES-H, 10 Glucose, 10 $CaCl_2$, 2.8 KCl, 2 $MgCl_2$, or as otherwise noted. The osmolarity was adjusted to 310 mOsm with mannitol, and pH was 7.2. The standard perforated patch solution contained (in mM); 135 CsGlutamate, 10 HEPES-H, 9.5 NaCl, 0.5 TEA-Cl, 0.53 amphotericin B; pH was 7.2 and osmolarity was 300 mOsm. Amphotericin B was prepared as described by Smith and Neher (1997). Pipettes were tip-dipped in amphotericin-free solution for 2–10 s, and back-filled with freshly mixed amphotericin-containing solution. The liquid junction potential between the extracellular Ringer and the intracellular solution was measured to be approximately 13 mV and all potentials were adjusted accordingly. All chemicals were obtained from Sigma Chemical company (St. Louis, MO) with the exception of CsOH (Aldrich, Milwaukee, WI), and amphotericin B (Calbiochem, La Jolla, CA), or as otherwise noted.

The standard whole-cell pipette solution contained (in mM); 145 CsGlutamate, 10 HEPES-Cs, 8 NaCl, 2 MgATP, 1 $MgCl_2$, 0.35 Na_2GTP (Boehringer Mannheim, Mannheim Germany), 0.1 fura-2 K^+ salt (Teflabs, Austin TX); pH was 7.2 and osmolarity was 300 mOsm. The solutions were further modified as indicated in the text for the different levels of buffered $[Ca^{2+}]_i$.

Electrochemical Measurements

Carbon fiber electrodes for amperometric catecholamine detection were prepared as in Smith and Neher (1997). The amperometric current was recorded using either an EPC-7 patch clamp amplifier (HEKA, Lambrecht Germany) or by the second headstage of a double EPC-9 amplifier (EPC-9/2, HEKA). Signals were either directly filtered at 1 kHz and sampled at 12 kHz by the EPC-9 or read from the EPC-7 and stored temporarily on a digital tape recorder to be later filtered at 1 kHz and resampled at 4 kHz using the continuous mode of Pulse.

Electrophysiological Measurements

Pipettes of approximately 2–3 MΩ resistance were pulled from borosilicate glass, partially coated with a silicone compound (G. E. Silicones, Bergen Op Zoom, The Netherlands), and lightly fire-polished. For acquisition we used an EPC-9 amplifier and PULSE software

running on an Apple Macintosh. Cm was estimated by the Lindau-Neher technique (for review, see Gillis, 1995) implemented as the "Sine + D. C." feature of the Pulse lock-in module. Either a 700 or 1000 Hz, 35 mV peak amplitude sinewave was applied to a holding potential of −83 mV and the reversal potential of the lock-in module was set to 0 mV. Data were acquired through a combination of the high time resolution PULSE software and the lower time resolution X-Chart plug-in module to the PULSE software. Briefly, membrane current was sampled at 10 kHz shortly (100 ms) before, during, and after the depolarizations, and Cm was calculated at either 0.7 or 1 kHz. Data acquired between high time resolution PULSE protocols were typically sampled at 12 Hz with the lower time resolution X-Chart plug-in.

Capacitance increases due to depolarizations were determined from the high time resolution Cm traces as the difference between mean Cm measured in a 50 ms window starting 50 ms after the depolarization minus the mean prestimulus Cm, also measured over a 50 ms window. The first 50 ms of the postdepolarization capacitance was neglected in order to avoid influences of nonsecretory capacitance transients (Horrigan and Bookman 1994). Experiments were carried out at 20°C–25°C.

Cytosolic Ca^{2+} Measurements

Cellular Ca^{2+} concentrations were measured in the perforated patch configuration by preincubating the cells in growth medium containing 1 μM of the membrane permeant acetyl methyl ester form of fura-2 (fura-2AM, Molecular Probes, Eugene OR; Grynkiewicz et al., 1985) for 10 min at 37°C. Following the experimental protocol, the perforated patch was ruptured causing the intracellular fura-2 to dialyze out of the cell, allowing for the measurement of the autofluorescence of the cell. The autofluorescence values at 360 and 390 nm wavelength excitation were subtracted from values measured during the experiment and the $[Ca^{2+}]$ was estimated after Grynkiewicz and colleagues (1985). In the whole-cell configuration, Ca^{2+} concentrations were estimated following dialysis of free fura-2 K^+ salt into the cell from the pipette and as further described by Neher (1989).

Computer Simulation of Measured RRP Recovery

A computer simulation of the measured RRP characteristics was based on the "Two Step Model of Secretion Control" (Heinemann et al., 1993). A brief summary of the model and its current implementation is supplied here. The two-step scheme for secretion describes the transition of vesicle between 3 separate states. Pool A is considered to be a large reserve pool of vesicles that mature, in a Ca^{2+}-dependent manner, into the release-ready vesicles of pool B. Vesicles in the B pool either revert and rejoin pool A, or undergo evoked Ca^{2+}-dependent secretion, described as the transition to pool C.

$$A \underset{k_{-1}}{\overset{k_1}{\rightleftharpoons}} B \xrightarrow{k_2} C \tag{3}$$

For the simulations, pool A was assumed to be equivalent to a number of vesicles totaling in capacitance to 5 pF (Heinemann et al., 1993). The forward rate constant k_1 between pools A and B is modeled as dependent upon $[Ca^{2+}]_i$ and is described by the Michaelis-Menten relationship in Equation 4;

$$k_1 = \frac{a_1 [Ca^{2+}]_i}{b_1 + [Ca^{2+}]_i} \tag{4}$$

where a_1 is the maximum possible value of k_1 and b_1 has the meaning of a K_D of a regulating site. In the simulations the stimulus-evoked $[Ca^{2+}]_i$ transient was approximated as a monoexponential decay from a maximum concentration, usually 1.2 μM, to a defined resting level (280 nM in the control case). The backward rate constant k_{-1} represents the spontaneous loss of vesicles from pool B to pool A. The rate of vesicle exocytosis, transition from pool B to C, is represented in the two-step model by the rate constant k_2 and is defined by Equation 5:

$$k_2 = a_3[Ca^{2+}]_i^3 \tag{5}$$

where a_3 is calculated from the data of Heinemann et al. (1994), according to the secretion study of Klingauf and Neher (1997) to be equal to 0.035 $\mu M^{-3} \cdot s^{-1}$. In this study a scheme assuming three sequential Ca^{2+} binding steps was used:

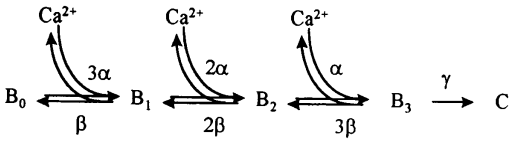

(6)

In order to derive the simple expression (Equation 3), it is assumed that at low $[Ca^{2+}]_i$ the state B_2 (i.e., the state of two Ca^{2+} ions bound to the Ca^{2+} sensor of a vesicle within pool B) is at equilibrium with free Ca^{2+}. This assumption is justified since the product $2 \cdot [Ca^{2+}]_i \cdot \alpha$ is small with respect to the backward rate 2β at sufficiently low $[Ca^{2+}]_i$. Therefore,

$$B_2 = B_0 \left(\frac{[Ca^{2+}]}{[Ca^{2+}] + K_D}\right)^2 \tag{7}$$

where K_D is the dissociation constant ($=\beta/\alpha$) of the Ca^{2+} sensor. The rate of exocytosis, r, is then given by the rate of reaching state B_3, multiplied by the probability, p_e, of an exocytosis event happening, once state B_3 has been reached;

$$r = \alpha[Ca^{2+}]_i B_2 p_e \tag{8}$$

with

$$p_e = \frac{\gamma}{\gamma + 3\beta} \tag{9}$$

where γ is the rate constant for exocytosis from the state B_3. We then obtain

$$r = B_0\left(\frac{[Ca^{2+}]}{[Ca^{2+}] + K_D}\right)^2 \alpha[Ca^{2+}]\frac{\gamma}{\gamma + 3\beta} \tag{10}$$

which, for $[Ca^{2+}]_i << K_D$ simplifies to

$$r = B_0\left(\frac{\gamma}{\gamma + 3\beta}\right)\left(\frac{\alpha^3}{\beta^2}\right)(Ca^{2+})^3 \tag{11}.$$

With the numerical values used by Klingauf and Neher (1997; i.e., $\alpha = 8\ \mu M^{-1}\ s^{-1}$, $p = 105\ s^{-1}$, $\gamma = 1000\ s^{-1}$), this results in the value for a_3 given above.

The $[Ca^{2+}]_i$-dependent steady-state size of pool B is described by Equation 12;

$$B_\infty = \frac{Ak_1}{(k_{-1} + k_2)} \tag{12}$$

where A is the size of pool A in farads. The time course for RRP recovery at a given, constant $[Ca^{2+}]_i$, is described by the equation

$$\tau = 1/(k_{-1} + k_2) \tag{13}$$

where τ represents the time constant of pool B recovery and the Ca^{2+} sensitivity is conferred through the Ca^{2+}-dependent rate constant k_2.

In order to estimate the poststimulus recovery of pool B, the differential equations derived from the model were solved using the Runge-Kutta integration method. Further characteristics of the simulation such as assumptions, constraints, and free parameters are described in the Results section.

Acknowledgments

We would like to thank Dr. Christian Rosenmund for critical comments on the manuscript. We thank F. Friedlein and M. Pilot for expert technical assistance. This work was supported by grants of the Deutsche Forschungsgemeinschaft (SFB 406, SFB 523, and CHV-113/65) and by the HFSP (RG-4/95B).

Received February 25, 1998; revised April 7, 1998.

References

Ämmälä, C., Eliasson, L., Bokvist, K., Berggren, P.-O., Honkanen, R. E., Sjöholm, Å., and Rorsman, P. (1994). Activation of protein kinases and inhibition of protein phosphatases play a central role in the regulation of exocytosis in mouse pancreatic b-cells. Proc. Natl. Acad. Sci. USA *91*, 4343–4347.

Bennett, M.K. (1997). Ca^{2+} and the regulation of neurotransmitter secretion. Curr. Opin. Neurol. *7*, 316–322.

Betz, W.J. (1970). Depression of transmitter release at the neuromuscular junction of the frog. J. Physiol. *206*, 629–644.

Bittner, M.A., and Holz, R.W. (1992). Kinetic analysis of secretion from permeabilized adrenal chromaffin cells reveals distinct components. J. Biol. Chem. *267*, 16219–16225.

Byrne, J.H., and Kandel, E.R. (1996). Presynaptic facilitation revisited: state and time dependence. J. Neurosci. *16*, 425–435.

Chow, R.H., and von Rüden, L. (1995). Chapter 11. Electrochemical detection of secretion from single cells. In Single-Channel Recording, 2nd Ed., B. Sakmann and E. Neher, eds. (New York: Plenum Press), pp. 245–275.

Deeney, J.T., Cunningham, B.A., Chheda, S., Bokvist, K., Juntti-Berggren, L., Lam, K., Korchak, H.M., Corkey, B.E., and Berggren, P.O. (1996). Reversible Ca^{2+}-dependent translocation of protein kinase C and glucose-induced insulin release. J. Biol. Chem. *271*, 18154–18160.

Delaney, K.R., Zucker, R.S., and Tank, D.W. (1989). Calcium in motor nerve terminals associated with posttetanic potentiation. J. Neurosci. *9*, 3558–3567.

del Castillo, J., and Katz, B. (1954). Quantal components of the end-plate potential. J. Physiol. *124*, 560–573.

Elmqvist, D., and Quastel, D.M.J. (1965). A quantitative study of end-plate potentials in isolated human muscle. J. Physiol. *178*, 505–529.

Fujita, Y., Sasaki, T., Fukui, K., Kotani, H., Kimura, T., Hata, Y., Südhof, T.C., Scheller, R.H., and Takai, Y. (1996). Phosphorylation of Munc-18/n-Sec1/rbSec1 by protein kinase C. J. Biol. Chem. *271*, 7265–7268.

Gerke, V., and Moss, S.E. (1997). Annexins and membrane dynamics. Biochem. Biophys. Acta *1357*, 129–154.

Gillis, K.D. (1995). Chapter 7. Techniques for membrane capacitance measurements. In Single-Channel Recording, 2nd Ed., B. Sakmann and E. Neher, eds. (New York: Plenum Press), pp. 155–198.

Gillis, K.D., Mößner, R., and Neher, E. (1996). Protein kinase C enhances exocytosis from chromaffin cells by increasing the size of the readily releasable pool of secretory granules. Neuron *16*, 1209–1220.

Greengard, P., Valtorta, F., Czernik, A.J., and Benfenati, F. (1993). Synaptic vesicle phosphoproteins and regulation of synaptic function. Science *259*, 780–785.

Grynkiewicz, G., Poenie, M., and Tsien, R. (1985). A new generation of Ca^{2+} indicators with greatly improved fluorescence properties. J. Biol. Chem. *260*, 3440–3450.

Hartwig, J.H., Thelen, M., Rosen, A., Janmey, P.A., Nairn, A.C., and Aderem, A. (1992). MARCKS is an actin filament crosslinking protein regulated by protein kinase C and calcium-calmodulin. Nature *356*, 618–622.

Heinemann, C., von Rüden, L., Chow, R.H., and Neher, E. (1993). A two-step model of secretion control in neuroendocrine cells. Pflügers Arch. *424*, 105–112.

Heinemann, C., Chow, R., Neher, E., and Zucker, R. (1994). Kinetics of the secretory response in bovine chromaffin cells following flash photolysis of caged Ca++. Biophys. J. *67*, 2546–2557.

Helmchen, F., Imoto, K., and Sakmann, B. (1996). Ca^{2+} buffering and action potential-evoked Ca^{2+} signaling in dendrites of pyramidal neurons. Biophys. J. *70*, 1069–1081.

Horrigan, F.T., and Bookman, R.J. (1994). Releasable pools and the kinetics of exocytosis in adrenal chromaffin cells. Neuron *13*, 1119–1129.

Kamiya, H., and Zucker, R.S. (1994). Residual Ca^{2+} and short-term synaptic plasticity. Nature *371*, 603–606.

Klingauf, J., and Neher, E. (1997). Modeling buffered Ca^{2+} diffusion near the membrane: implications for secretion in neuroendocrine cells. Biophys. J. *72*, 674–690.

Knight, D.E., and Baker, P.F. (1983). The phorbol ester TPA increases the affinity of exocytosis for calcium in 'leaky' adrenal medullary cells. FEBS Lett. *160*, 98–100.

Kretz, R., Shapiro, E., and Kandel, E.R. (1982). Post-tetanic potentiation at an identified synapse in Aplysia is correlated with a Ca^{2+}-activated K^+ current in the presynaptic neuron: evidence for a Ca^{2+} accumulation. Proc. Natl. Acad. Sci. USA *79*, 5430–5434.

Kusano, K., and Landau, E.M. (1975). Depression and recovery of transmission at the squid giant synapse. J. Physiol. *245*, 13–32.

Liley, A.W., and North, K.A.K. (1953). An electrical investigation of effects of repetitive stimulation on mammalian neuromuscular junction. J. Neurophysiol. *16*, 509–527.

Moser, T., and Neher, E. (1997). Rapid exocytosis in single chromaffin cells recorded from mouse adrenal slices. J. Neurosci. *17*, 2314–2323.

Neher, E. (1989). Combined fura-2 and patch clamp measurements in rat peritoneal mast cells. In Neuromuscular Junction, L.C. Sellin, R. Libelius, and S. Thesleff, eds. (Amsterdam: Elsevier), pp. 65–76.

Neher, E., and Augustine, G.J. (1992). Calcium gradients and buffers in bovine chromaffin cells. J. Physiol. *450*, 273–301.

Neher, E., and von Rüden, L. (1994). Depression and augmentation of quantal release in adrenal chromaffin cells. Adv. Second Messenger Phosphoprotein Res. *29*, 353–362.

Neher, E., and Zucker, R.S. (1993). Multiple calcium-dependent processes related to secretion in bovine chromaffin cells. Neuron *10*, 21–30.

Nishizaki, T., Walent, J.H., Kowalchyk, J.A., and Martin, T.F. (1992). A key role for a 145-kDa cytosolic protein in the stimulation of Ca(2+)-dependent secretion by protein kinase C. J. Biol. Chem. *267*, 23972–23981.

Oheim, M., Loerke, D., Stümer, W., and Chow, R. (1998). The last few seconds in the life of a secretory granule. Eur. Biophys. J. *27*, 83–98.

Parsons, T.D., Coorssen, J.R., Horstmann, H., and Almers, W. (1995). Docked granules, the exocytic burst, and the need for ATP hydrolysis in endocrine cells. Neuron *15*, 1085–1096.

Plattner, H., Artalejo, A., and Neher, E. (1997). Ultrastructural organization of bovine chromaffin cell cortex—analysis by cryofixation and morphometry of aspects pertinent to exocytosis. J. Cell Biol. *139*, 1709–1717.

Sarafian, T., Pradel, L.A., Henry, J.P., Aunis, D., and Bader, M.F. (1991). The participation of annexin II (calpactin I) in calcium-evoked exocytosis requires protein kinase C. J. Cell Biol. *114*, 1135–1147.

Seward, E.P., and Nowycky, M.C. (1996). Kinetics of stimulus-coupled secretion in dialyzed bovine chromaffin cells in response to trains of depolarizing pulses. J. Neurosci. *16*, 553–562.

Seward, E.P., Chernevskaya, N.I., and Nowycky, M.C. (1995). Exocytosis in peptidergic nerve terminals exhibits two calcium-sensitive phases during pulsatile calcium entry. J. Neurosci. *15*, 3390–3399.

Shimazaki, Y., Nishiki, T., Omori, A., Sekiguchi, M., Kamata, Y., Kozaki, S., and Takahashi, M. (1996). Phosphorylation of 25-kDa synaptosome-associated protein. J. Biol. Chem. *271*, 14548–14553.

Smith, C., and Neher, E. (1997). Multiple forms of endocytosis in bovine adrenal chromaffin cells. J. Cell Biol. *139*, 885–894.

Stevens, C.F., and Tsujimoto, T. (1995). Estimates for the pool size of releasable quanta at a single central synapse and for the time required to refill the pool. Proc. Natl. Acad. Sci. USA *92*, 846–849.

Steyer, J.A., Horstmann, H., and Almers, W. (1997). Transport, docking and exocytosis of single secretory granules in live chromaffin cells. Nature *388*, 474–478.

TerBush, D.R., Bittner, M.A., and Holz, R.W. (1988). Ca^{2+} influx causes rapid translocation of protein kinase C to membranes. Studies of the effects of secretagogues in adrenal chromaffin cells. J. Biol. Chem. *263*, 18873–18879.

Thomas, P., Wong, J.G., Lee, A.K., and Almers, W. (1993). A low affinity Ca^{2+} receptor controls the final steps in peptide secretion from pituitary melanotrophs. Neuron *11*, 93–104.

Vitale, M.L., Seward, E.P., and Trifaró, J.-M. (1995). Chromaffin cell cortical actin network dynamics control the size of the release-ready vesicle pool and the initial rate of exocytosis. Neuron *14*, 353–363.

von Gersdorff, H., and Matthews, G. (1997). Depletion and replenishment of vesicle pools at a ribbon-type synaptic terminal. J. Neurosci. *17*, 1919–1927.

von Gersdorff, H., Schneggenburger, R., Weis, S., and Neher, E. (1997). Presynaptic depression at a Calyx synapse: the small contribution of metabotropic glutamate receptors. J. Neurosci. *17*, 8137–8146.

von Rüden, L., and Neher, E. (1993). A Ca-dependent early step in the release of catecholamines from adrenal chromaffin cells. Science *262*, 1061–1065.

Zhou, Z., and Neher, E. (1993). Mobile and immobile calcium buffers in bovine adrenal chromaffin cells. J. Physiol. *469*, 245–273.

Zucker, R.S. (1996). Exocytosis: a molecular and physiological perspective. Neuron *17*, 1049–1055.

Zucker, R.S., Delaney, K.R., Mulkey, R., and Tank, D.W. (1991). Presynaptic calcium in transmitter release and posttetanic potentiation. Ann. NY Acad. Sci. *635*, 191–207.